Chapter 4
Swift-Hohenberg Equation

4.1 Cellular Patterns

Figure 4.1 exhibits spatial structures which can be observed in experiments on Rayleigh-Bénard convection [15]. They emerge without special interference from the outside as well-ordered spatial structures, which reminds one on two dimensional crystalline structures. However, in contrast to solid state crystals, they are formed under nonequilibrium conditions and can exhibit quite interesting phenomena since they are not ruled by the rather restricting fundamental laws of thermodynamics. Important questions concern the processes underlying the determination of
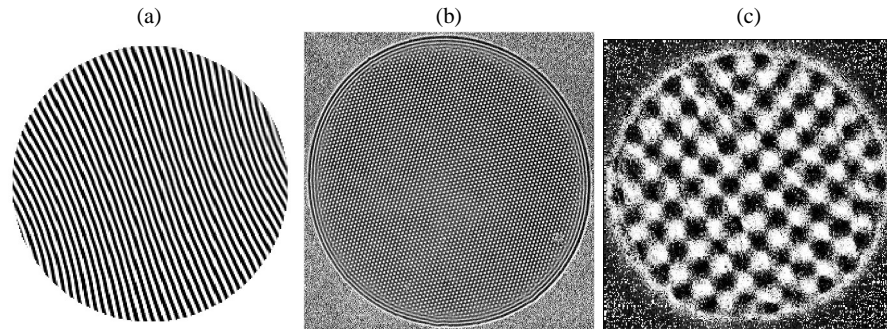

Fig. 4.1 Convection patterns. (a) Rolls; (b) Hexagons; (c) Squares.

the wavelength of the patterns and the selection of the planform, i.e. the question, what type of crystal structure eventually emerges. Furthermore, Fig. 4.2 (a) demonstrates the existence of patterns with nontrivial topology generated by defects in the roll structures [15]. The fact that Rayleigh-Bénard convection is a far from equilibrium phenomena manifests itself in the observation of patterns, which permanently undergo temporal evolution without approaching a final, stationary pattern.
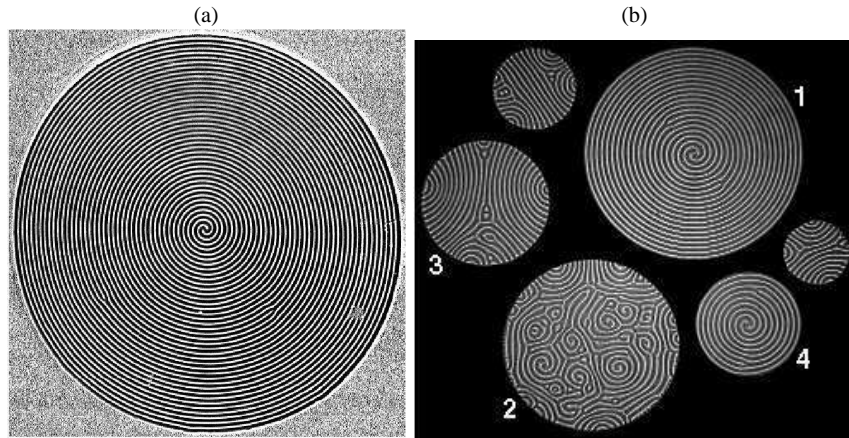
Fig. 4.2 Convection patterns: (a) Giant spiral patterns; (b) From single spirals to spiral turbulence.

The corresponding temporal patterns can become rather complicated. An example of the so-called spiral turbulence state is depicted in Fig. 4.2 (b). It is a challenge to understand the physical processes leading to permanently evolving structures, their spatial and topological properties.

4.2 The Order Parameter Concept

The mentioned patterns arising in Rayleigh-Bénard convection are only few selected examples from the world of nonequilibrium pattern forming systems. Experiments and their theoretical explanations suggest the existence of universal phenomena, i.e. similar pattern forming processes arising in quite different systems ranging from laser physics, hydrodynamics, reaction diffusion systems to biological systems. This means that phenomena of spontaneous pattern formation in nonequilibrium systems can be described on the basis of the same mathematical structures irrespective of the specific properties of the considered systems.

From a physical point of view the universal features of pattern formation can be summarized in the *order parameter concept*. A detailed analysis of pattern forming systems reveals that pattern formation is goverend by *order parameters*, whose spatio-temporal behaviour is determined by nonlinear partial differential equations. Quite different systems, e.g. reaction diffusion systems or convection experiments, are governed by the same order parameter dynamics. The validity of the order parameter concept can be assessed for systems in the vicinity of instabilities starting from the basic mathematical formulation of the system under consideration. For a detailed discussion we refer the reader to the literature (e.g. [30], [24], [33]).

The order parameter concept is a generalization of the Ginzburg- Landau theory of phase transitions in equilibrium systems. We consider a pattern forming system

described by a state vector $\mathbf{q}(\mathbf{r},t)$, which consists e.g. of the velocity field, the temperature field and the pressure in the case of Rayleigh Bénard system. It obeys an evolution equation in forms of partial differential equation

$$\partial_t \mathbf{q}(\mathbf{r},t) = \mathbf{N}[\nabla, \mathbf{q}(\mathbf{r},t)]. \tag{4.1}$$

These are, e.g. the basic fluid dynamical equations. The basic equations for laser instabilities are the Maxwell-Bloch equations for a state vector consisting of the electric field, inversion, and polarization of the laseractive medium.

The long term behaviour of the state vector $\mathbf{q}(\mathbf{r},t)$ of a system undergoing a process of pattern formation can be represented as a functional of one or several *order parameters*, denoted by $\psi(t)$

$$\mathbf{q}(\mathbf{r},t) = \mathbf{Q}[\psi(\mathbf{r},t)]. \tag{4.2}$$

Instead of solving the determining equations for the state vector $\mathbf{q}(\mathbf{r},t)$ the spatio-temporal behaviour is determined by an evolution equation for the order parameter $\psi(\mathbf{r},t)$

$$\partial_t \psi(\mathbf{r},t) = h[\psi(\mathbf{r},t)]. \tag{4.3}$$

Quite often, the order parameter can directly be related to a physical observable. In the case of the Rayleigh-Bénard experiment we can identify the order parameter $\psi(\mathbf{x},t)$ as the temperature field in a horizontal plane in the convection box. For laser systems exhibiting pattern formation in the transverse field the order parameter is related to the electric field amplitude. The validity of the order parameter concept can be proofed for systems close to instabilities, where the system's behaviour changes qualitatively. In these situations the order parameter can be identified and the corresponding order parameter dynamics can be derived from the basic evolution equations. On the other hand, the order parameter dynamics quite often can be established relying on phenomenological arguments combined with symmetry considerations.

Let us briefly exemplify the order parameter concept for the case of Rayleigh-Bénard convection. The velocity field $\mathbf{u}(\mathbf{x},t)$ and the deviations $\Theta(\mathbf{x},t)$ from a basic linear temperature profile can be represented as

$$\Theta(x,y,z,t) = \psi(x,y,t)\,\sin z + \mathcal{O}(\psi^2). \tag{4.4}$$

A similar expression holds for the velocity field. The fields consist, up to higher order terms with respect to the order parameter field, of a product of the two dimensional order parameter field $\psi(\mathbf{x},t)$ and a z-dependent profile. In case that

$$\psi(x,y,t) = a(t)\,\sin(kx+\varphi_0) = A(t)\,e^{ikx}+c.c. \tag{4.5}$$

with a certain wave number k, the field describes convective rolls with wavelenght $\lambda = 2\pi/k$. It can be shown that close to instability the complex amplitude $A(t)$ obeys the nonlinear differential equation

$$\dot{A}(t) = \varepsilon A(t) - |A(t)|^2 A(t), \tag{4.6}$$

where ε is a measure of the deviation of the temperature difference across the lower and upper plates from the critical one and serves as control parameter. For $\varepsilon > 0$ the purely heat conductive state $a = 0$ becomes unstable and the amplitude $|A| = \pm\sqrt{\varepsilon}$ approaches a stationary value. The solution corresponds to a perfectly aligned stripe pattern, analogous to a perfect two-dimensional crystal.

If the stripe patterns are slightly modulated in space, the complex amplitude A is a spatially dependent quantity, $A(x,y,t)$. It can be shown that this amplitude obeys an evolution equation of the form

$$\partial A(x,y,t) = \left[\varepsilon + \left(\frac{\partial}{\partial x} - \frac{i}{\sqrt{2}}\frac{\partial^2}{\partial y^2}\right)^2\right] A(x,y,t) - |A(x,y,t)|^2 A(x,y,t). \tag{4.7}$$

This equation allows one to study stripe patterns with *defects* as well as so-called *long wave instabilities* of stripe patterns. It is denoted as Newel-Whitehead-Segel equation.

Hexagonal patterns are obtained by a superposition of stripe patterns. In this case the temperature field takes the form

$$\Theta(\mathbf{x},t) = \sum_{i=1}^{3} A_i e^{i\mathbf{k}_i \cdot \mathbf{x}} \sin(\pi z) + h.o.t. \tag{4.8}$$

and the amplitudes obey coupled Newel-Whitehead-Segel equations. Equations for spatially varying amplitudes allows one to describe the processes of planform selection, the behaviour deformed patterns in the presence of defects and fronts between, e.g. stripe patterns and hexagonal patterns.

Finally, natural patterns, i.e. patterns consisting of patches of differently oriented stripe patterns including defects, fronts etc. are captured by the spatio-temporal evolution of the full order parameter field $\psi(\mathbf{x},t)$. In general, the evolution equation for the order parameter field $\psi(x,y,t)$ takes the form

$$\partial_t \psi(\mathbf{x},t) = L(\Delta)\psi(\mathbf{x},t) + N[\psi(\mathbf{x},t)] \tag{4.9}$$

where the linear operator $L(\Delta)$ and the nonlinear functional $N[\psi(\mathbf{x},t)]$ can be of a complicated form. In general studies of pattern forming processes, they are simplified, leading to *model equations*, which frequently are denoted as Swift-Hohenberg equations. Here, the nonlinear functional $N[\psi(\mathbf{x},t)]$ is approximated by polynomials of ψ and their low order derivatives.

4.3 Order Parameter Equation

The Swift-Hohenberg equation describes the spatio-temporal evolution of a real order parameter field $\psi(\mathbf{x},t)$ and takes the form

$$\partial_t \psi(\mathbf{x},t) = \left[\varepsilon - \left(k_c^2 + \Delta\right)^2\right] \psi(\mathbf{x},t) + \delta \psi(\mathbf{x},t)^2 - \psi(\mathbf{x},t)^3. \qquad (4.10)$$

Additionally, one has to formulate suitable boundary conditions. Usually, one assumes the existence of periodic boundary conditions

$$\begin{aligned} \psi(x,y,t) &= \psi(x+L,y,t), \\ \psi(x,y,t) &= \psi(x,y+L,t). \end{aligned} \qquad (4.11)$$

However, as we shall see, boundaries have a strong influence on the global organization of the patterns.

Furthermore, it is important to notice that the Swift-Hohenberg equation (4.10) is invariant with respect to rotations of the coordinate system, as well as reflections.

From a qualitative point of view the Swift-Hohenberg equation as an order parameter equation can be motivated on the basis of the following facts.

4.3.0.1 Instability and Linear Growth of Modes

The patterns show the occurrence of a certain wavelenght. Decomposing the order parameter field into plane waves

$$\psi(\mathbf{x},t) = \sum_{\mathbf{k}} A_{\mathbf{k}}(t) \frac{1}{\sqrt{V}} e^{i\mathbf{k}\cdot\mathbf{x}} \qquad (4.12)$$

we have to specify the temporal behaviour of the amplitudes $A_{\mathbf{k}}(t)$. Since we restrict ourselves for the time being to linear evolution, this behaviour is exponential:

$$A_{\mathbf{k}}(t) = e^{\lambda(\mathbf{k})t} A_{\mathbf{k}}(0). \qquad (4.13)$$

The growth rates should be positive for amplitudes with $|\mathbf{k}| \approx k_c$, whereas for other amplitudes it should be negative. Due to rotational symmetry it is a function of $k = ||\mathbf{k}||$. These properties are taken into account by the ansatz

$$\lambda(\mathbf{k}) = \varepsilon - \left[k_c^2 - \mathbf{k}^2\right]^2. \qquad (4.14)$$

The growth rate depends on the wave vector $\mathbf{k}$. It is depicted in Fig. (**??**) for the cases $\varepsilon < 0$ and $\varepsilon > 0$. For $\varepsilon < 0$ the growth rate for values of k are negative and the order parameter $\psi(\mathbf{x},t)$ tends to zero under the evolution of the linear equation (4.13). For $\varepsilon > 0$ disturbances with wave vectors $\mathbf{k}$ with absolute value $k \approx k_c$ get positive growth rates $\lambda(k)$ indicating that the corresponding modes grow exponentially in time.

We consider a two dimensional domain. Then all modes with $\mathbf{k}$-vectors with absolute value taken from a ring of width $\approx \sqrt{\varepsilon}$ close to k_c are unstable. The solution of the linear equation would be a superposition of all these modes given by the initial condition

$$\psi(\mathbf{x},t) = \sum_{\mathbf{k}} A(\mathbf{k},0)\frac{1}{\sqrt{V}}e^{i\mathbf{k}\cdot\mathbf{x}}e^{\lambda(k)t}. \tag{4.15}$$

Finally, we can summarize the evolution equation for the order parameter field. Transforming to real space we obtain

$$\dot{\psi}(\mathbf{x},t) = \left[\varepsilon - \left[k_c^2 + \Delta\right]^2\right]\psi(\mathbf{x},t). \tag{4.16}$$

4.3.0.2 Nonlinear Saturation and Selection of Patterns

The linear growth of modes (4.13) is modified leading to a saturation of the amplitudes. In a naive way, one can extend the differential equation determining the amplitudes by the inclusion of a nonlinear term

$$\dot{A}_{\mathbf{k}}(t) = \left[\varepsilon - \left[k_c^2 - \mathbf{k}^2\right]^2\right]A_{\mathbf{k}}(t) - |A_{\mathbf{k}}(t)|^2 A_{\mathbf{k}}(t). \tag{4.17}$$

This would lead to the saturation of the amplitudes with positive growth rates in the long term limit

$$|\xi_{\mathbf{k}}(t)|^2 = \left[\varepsilon - \left[k_c^2 - \mathbf{k}^2\right]^2\right], \tag{4.18}$$

whereas modes with negative growth rate die out. However, there is non interaction between amplitudes with different values of $\mathbf{k}$. Physically, this means that the process of *pattern selection* is missing.

In order to include the phenomenon of pattern selection we are led to consider the general cubic terms

$$\dot{A}_{\mathbf{k}}(t) = \lambda(\mathbf{k})A_{\mathbf{k}}(t) - \sum_{\mathbf{k}_1,\mathbf{k}_2,\mathbf{k}_3} \delta_{\mathbf{k};\mathbf{k}_1+\mathbf{k}_2+\mathbf{k}_3}\gamma_{\mathbf{k};\mathbf{k}_1,\mathbf{k}_2,\mathbf{k}_3}A_{\mathbf{k}_1}(t)A_{\mathbf{k}_2}(t)A_{\mathbf{k}_3}(t), \tag{4.19}$$

where the mode coupling coefficients $\gamma_{\mathbf{k};\mathbf{k}_1,\mathbf{k}_2,\mathbf{k}_3}$ have to be choosen appropriately. The δ-function arises due to the fact that we consider patterns in systems with translational symmetry: Provided $\psi(\mathbf{x},t)$ is a solution of the evolution equation, the shifted pattern

$$\psi(\mathbf{x}-\mathbf{X},t) = \sum_{\mathbf{k}} A_{\mathbf{k}}(t)e^{i\mathbf{k}\cdot(\mathbf{x}-\mathbf{X})} \tag{4.20}$$

has to be a possible solution, too. As a consequence, the amplitude equations have to be invariant with respect to the transformation

$$A_{\mathbf{k}}(t) \to A_{\mathbf{k}}(t)e^{-i\mathbf{k}\cdot\mathbf{X}}. \tag{4.21}$$

As a consequence, each amplitude equation

$$\dot{A}_{\mathbf{k}} = \lambda(\mathbf{k})A_{\mathbf{k}} + N_{\mathbf{k}}[\{A_k\}] \tag{4.22}$$

has to obey the following relation:

$$N_{\mathbf{k}}[\{A_k\}] = e^{i\mathbf{k}\cdot\mathbf{X}} N_{\mathbf{k}}[\{e^{-i\mathbf{k}\cdot\mathbf{X}} A_k\}]. \tag{4.23}$$

It requires the presence of the δ- function in (4.19). Equation (4.23) is an example of an *equivariance condition*, i.e. a condition which is related to underlying symmetries.

Now we consider a further simplification. We restrict ourselves patterns, which are formed by amplitudes with absolute value of the wave vector $|\mathbf{k}| = k_c$:

$$\psi(\mathbf{x},t) = \sum_{\mathbf{k},|\mathbf{k}|=k_c} A_{\mathbf{k}}(t) e^{i\mathbf{k}\cdot\mathbf{x}} + c.c. \tag{4.24}$$

In principle, the evolution equation (4.19) introduces couplings to further amplitudes with $|\mathbf{k}| \neq k_c$. These amplitudes are assumed to be weakly excited and are simply neglected. The temporal evolution is considered on the basis of the truncated evolution equation (4.19).

According to (4.19) the δ-function in the nonlinearity couple amplitudes, whose wave vectors form an equilateral parallelogram. The combinations summarized in table below

$\mathbf{k}$	$\mathbf{k}_1$	$\mathbf{k}_2$	$\mathbf{k}_3$
$\mathbf{k}$	$\mathbf{k}_1$	$-\mathbf{k}_1$	$\mathbf{k}$
$\mathbf{k}$	$\mathbf{k}_1$	$\mathbf{k}$	$-\mathbf{k}_1$
$\mathbf{k}$	$\mathbf{k}$	$\mathbf{k}_1$	$-\mathbf{k}_1$

can arise.

As a consequence, we can rewrite the amplitude equations in the form

$$\dot{A}_{\mathbf{k}} = \lambda(k) A_{\mathbf{k}} - S|A_{\mathbf{k}}|^2 A_{\mathbf{k}} - A_{\mathbf{k}} \sum_{\mathbf{k}'\neq\mathbf{k}} W_{\mathbf{k},\mathbf{k}'}|A_{\mathbf{k}'}|^2. \tag{4.25}$$

Thereby, we have the relation

$$S = \gamma_{\mathbf{k};\mathbf{k},\mathbf{k},-\mathbf{k}} + \gamma_{\mathbf{k};\mathbf{k},-\mathbf{k},\mathbf{k}} + \gamma_{-\mathbf{k};\mathbf{k},\mathbf{k},\mathbf{k}},$$
$$W_{\mathbf{k},\mathbf{k}'} = \gamma_{\mathbf{k};\mathbf{k},\mathbf{k}',-\mathbf{k}'} + \gamma_{\mathbf{k};\mathbf{k}',\mathbf{k},-\mathbf{k}'} + \gamma_{-\mathbf{k};\mathbf{k}',-\mathbf{k}',\mathbf{k}}. \tag{4.26}$$

The coupling coefficient $W_{\mathbf{k},\mathbf{k}'}$ depend on the angle φ between the wave vectors with $\mathbf{k}, \mathbf{k}'$:

$$W_{\mathbf{k},\mathbf{k}'} = W(\varphi). \tag{4.27}$$

We can now make a further distinction based on symmetry argument. If we consider systems with reflectionel symmetry we should have the invariance

$$W(\varphi) = W(\varphi), \tag{4.28}$$

$$W_{\mathbf{k},\mathbf{k}'} = W(\mathbf{k}\cdot\mathbf{k}'). \tag{4.29}$$

For patterns in systems with broken reflectional symmetry

$$W_{\mathbf{k},\mathbf{k}'} = W(\mathbf{k}\cdot\mathbf{k}', \mathbf{e}_z\cdot[\mathbf{k}\times\mathbf{k}']) \tag{4.30}$$

an additional dependency on $\mathbf{e}_z\cdot[\mathbf{k}\times\mathbf{k}']$ has to be taken into account.

4.3.0.3 Square Lattice

Let us consider the case of a square lattice. Then we have the amplitudes

$$\xi_{k,0},\ \xi_{-k,0}=\xi_{k,0}^*,\ \xi_{0,k},\ \xi_{0,-k}=\xi_{0,k}^*. \tag{4.31}$$

The amplitude equations read

$$\dot{\xi}_{k,0} = \lambda\xi_{k,0} - S\xi_{k,0}|\xi_{k,0}|^2 - W\xi_{k,0}|\xi_{0,k}|^2,$$
$$\dot{\xi}_{0,k} = \lambda\xi_{0,k} - S\xi_{0,k}|\xi_{0,k}|^2 - W\xi_{0,k}|\xi_{k,0}|^2. \tag{4.32}$$

Let us now consider explicity examples: The mode coupling coefficient for the nonlinearity $\psi^3(\mathbf{x},t)$ is given by

$$\Gamma_{\mathbf{k};\mathbf{k}_1,\mathbf{k}_2,\mathbf{k}_3} = \int d\mathbf{x}\frac{e^{i[-\mathbf{k}+\mathbf{k}_1+\mathbf{k}_2+\mathbf{k}_3]\mathbf{x}}}{V^2}\xi_{\mathbf{k}_1}(t)\xi_{\mathbf{k}_2}(t)\xi_{\mathbf{k}_3}(t)$$
$$= \frac{1}{V}\delta_{\mathbf{k},\mathbf{k}_1+\mathbf{k}_2+\mathbf{k}_3}\xi_{\mathbf{k}_1}(t)\xi_{\mathbf{k}_2}(t)\xi_{\mathbf{k}_3}(t) \tag{4.33}$$

and we obtain

$$S = \frac{3}{V}, \qquad W_{\mathbf{k},\mathbf{k}'} = S. \tag{4.34}$$

As we shall see the special form of the nonlinearity decides about the selection of the patterns.

Square patterns are obtained from the nonlinearity

$$N[\psi] = \nabla\cdot\left[\psi\left(\nabla\psi\right)^2\right]. \tag{4.35}$$

The corresponding equation is denoted as Gertsberg- Shivashinsky equation and can be derived for large aspect ratio Rayleigh Bénard systems in the presence of poorly heat conductive states.

In the following we shall consider order parameter equations of the form

$$\dot{\psi}(\mathbf{x},t) = \left[\varepsilon - \left(k_c^2 + \Delta\right)^2\right]\psi(\mathbf{x},t) + N[\psi]. \tag{4.36}$$

Here $N[\psi]$ denotes a nonlinear functional of the order parameter field $\psi(\mathbf{x},t)$. A discussion of the order parameter equations can be found in [6].

4.4 Variational Versus Nonvariational Equations

The Swift-Hohenberg equation (4.10) can be expressed in variational form (see App. E)

$$\dot{\psi}(\mathbf{x},t) = -\frac{\delta}{\delta\psi(\mathbf{x},t)} V\left[\psi(\mathbf{x},t)\right] \qquad (4.37)$$

with the Ljapunov functional

$$V = \int d\mathbf{x}\left\{\frac{1}{2}\left[(k_c^2+\Delta)\psi(\mathbf{x},t)\right]^2 - \frac{\varepsilon}{2}\psi(\mathbf{x},t)^2 + \frac{1}{4}\psi(\mathbf{x},t)^4\right\} - \frac{\delta}{3}\psi(\mathbf{x},t)^3. \qquad (4.38)$$

This is an important property since the stable stationary states are determined by the local minima of this functional. The existence of a Ljapunov functional yields properties which are well-known from systems in thermal equilibrium. States of equilibrium systems are extremal states of a thermodynamic potential, e.g. the free energy. Similarly, patterns of a nonequilibrium systems having a Ljapunov functional are determined by the minima of this functional. However, we shall point out that this functional may have a great variety of different minima. This makes the study of such systems highly interesting. Furthermore, we may consider order parameter equations, which can not be expressed in variational form. As we shall see this will lead us to models exhibiting spatio-temporal chaos.

4.5 Numerical Treatment: Pseudo-Spectral Methods

Numerically, the Swift-Hohenberg equation (4.10) can be solved in a straight forward manner by the pseudo-spectral method.

4.5.1 Periodic Boundaries

For the numerical treatment of the order parameter equation (4.36) one could convert it into a set of amplitude equations of the form (4.19). However, the evaluation of the sum over the mode coupling coefficients would be extremely time consuming. In this case, the use of a pseudo-spectral methods is straight forward.

Fourier transform of the Swift-Hohenberg equation leads to

$$\dot{\psi}(\mathbf{k},t) = L(-k^2)\psi(\mathbf{k},t) + N(\mathbf{k},t), \qquad (4.39)$$

where $N(\mathbf{k},t)$ denotes the Fourier transform of the nonlinearity. For the standard nonlinearity we explicitly obtain

$$N(\mathbf{k},t) = \frac{1}{\sqrt{V}}\int d\mathbf{x}e^{-i\mathbf{k}\cdot\mathbf{x}}\left[\delta\psi(\mathbf{x},t)^2 - \psi(\mathbf{x},t)^3\right]. \qquad (4.40)$$

The following time stepping scheme turns out to be sufficient for most purposes:

$$\frac{1}{\tau}\left[\psi(\mathbf{k},t+\tau)-\psi(\mathbf{k},t)\right]=L(-k^2)\,\psi(\mathbf{k},t+\tau)+N(\mathbf{k},t)\,. \qquad (4.41)$$

Explicitly,

$$\psi(\mathbf{k},t+\tau)=\frac{1}{1/\tau-L(-k^2)}\left[\frac{\psi(\mathbf{k},t)}{\tau}+N(\mathbf{k},t)\right]\,. \qquad (4.42)$$

4.5.2 Inclusion of Boundaries

The pseudo-spectral method is designed for the treatment of patterns for domains in the presence of periodic boundary conditions. However, a variety of pattern forming properties depend on the geometry of the considered domain and the corresponding boundary conditions.

An elegant method to introduce boundaries consist of the inclusion of so-called ramps. The idea of a ramp is also utilized in experiments. In Rayleigh-Bénard convection this would simply correspond to a nonuniform heating of the layer from below in such a way that the system becomes subcritical outside a certain domain. Numerically, this can be achieved by introducing a space-dependent control parameter

$$\varepsilon=\varepsilon_0+\varepsilon_1(\mathbf{x})\,. \qquad (4.43)$$

The contribution $\varepsilon_1(\mathbf{x})$ is negative outside the domain under consideration leading to a damping of the patterns in the outer region. The computation can then be performed using periodic boundary conditions. The only change now consists in the replacement of $N[\psi(\mathbf{x},t)$ with

$$\tilde{N}(\psi(\mathbf{x},t))=N(\psi(\mathbf{x},t))+\varepsilon_1(\mathbf{x})\psi(\mathbf{x},t) \qquad (4.44)$$

and the iterative scheme reads

$$\psi(\mathbf{k},t+\tau)=\frac{1}{1/\tau-L(-k^2)}\left[\frac{\psi(\mathbf{k},t)}{\tau}+\tilde{N}(\mathbf{k},t)\right]\,, \qquad (4.45)$$

where $\tilde{N}(\mathbf{k},t)$ is the Fourier transform of $\tilde{N}(\psi(\mathbf{x},t))$.

The introduction of a ramp is a special case of so-called penalty methods. We emphasize that, especially in convection experiments, the proper treatment of boundaries is a rather delicate subject.

4.6 Stripes

Figure 4.3 exhibits the temporal evolution of the solution of Swift-Hohenberg equation ($\delta = 0$) starting from random initial conditions

$$\psi(\mathbf{x},t) = \psi(\mathbf{x},0)\,, \tag{4.46}$$

where $\psi(\mathbf{x},0)$ is a random number from taken from the interval $-\sqrt{\varepsilon} \leq \psi(\mathbf{x},0) \leq \sqrt{\varepsilon}$. One observes the selection of *stripes*. However, the evolving pattern contains dislocations and grain boundaries between regions with differently oriented stripes. The parameter set used in the simulation is

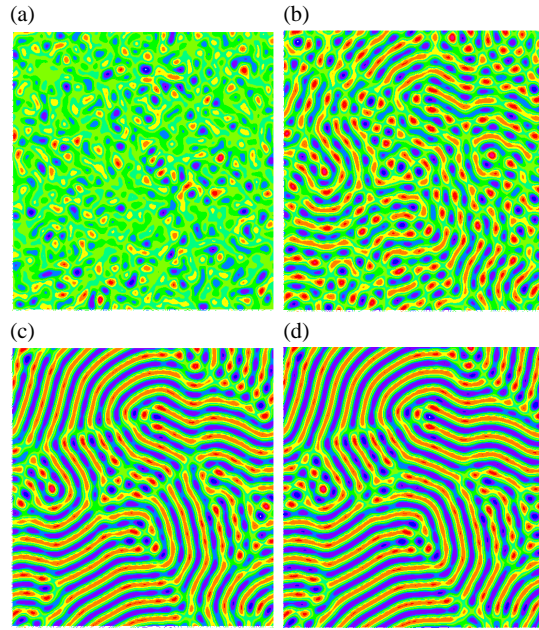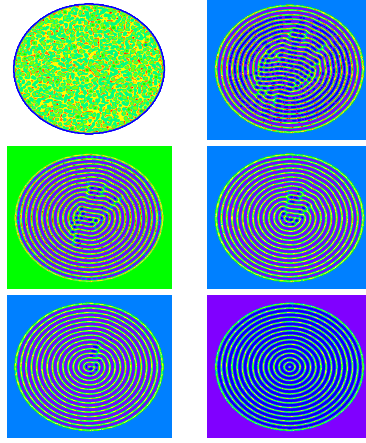| Figure	Fig. 4.3
Control parameter	$\varepsilon = 0.3$, $\delta = 0.0$
Domain size L	100
Time step τ	0.01
Number of grid points	256×256
Initial condition	random

Fig. 4.3 Numerical calculation of the evolution of stripe patterns from the Swift-Hohenberg equation (4.10) ($\delta = 0$, $\varepsilon = 0.3$)

Figure	Fig. (**??**)
Control parameter	ε=0.3, δ=0.0
Domain size L	100
Time step τ	0.01
Number of grid points	256×256
Initial condition	random

Fig. 4.4 Numerical Calculation of the evolution of stripe patterns from the Swift-Hohenberg equation (4.10) ($\delta = 0$, $\varepsilon = 0.3$). Patterns evolve in a circular domain using a ramp.

4.6.1 Amplitude Equation for Stripes

We now calculate the solution of the stripe patterns analytically. To this end we consider $\delta = 0$ and perform the ansatz

$$\psi(\mathbf{x},t) = A(t)\,e^{ik_0x} + c.c.. \tag{4.47}$$

In this representation, the amplitude A is a function of time. Inserting this ansatz into the Swift-Hohenberg equation one obtains

$$[\dot{A} - \varepsilon A + 3A|A|^2]e^{ik_0x} = -A^3 e^{3ik_0x} - 3A^*|A|^2 e^{-3ik_0x} + c.c.. \tag{4.48}$$

We see that our ansatz produces terms proportional to e^{3ik_0x} indicating that the ansatz (4.47) is not sufficient and should be extended to include higher terms

$$\psi(\mathbf{x},t) = A(t)\,e^{ik_0x} + A_3(t)\,e^{i3k_0x} + A_5(t)\,e^{i5k_0x} \ldots + c.c.. \tag{4.49}$$

However, if one assumes that the higher order amplitudes are smaller than the leading amplitude A, one can determine A from the amplitude equation

$$\partial_t A = (\varepsilon - (k_c^2 - k_0^2)^2)A - 3A|A|^3. \tag{4.50}$$

There are stripe solutions

$$A = \sqrt{\frac{\varepsilon - (k_c^2 - k_0^2)^2}{3}}\, e^{-i\varphi} \tag{4.51}$$

provided the growth rate $\varepsilon - (k_c^2 - k_0^2)^2$ is positive. As a result of translational symmetry the phase of the complex amplitude is undetermined.

However, as we shall discuss in the next subsection, the stripe solutions (4.51) are not stable for an arbitray wave number k_0. There are long-wave instabilities.

4.6.2 Envelope Equation

We extend our treatment to the case, where the amplitude is a slowly varying function of $\mathbf{x}$. Since we can include deviations from the wave number in the amplitude $A(\mathbf{x},t)$, we can choose $k_0 = k_c$:

$$\psi(\mathbf{x},t) = A(\mathbf{x},t)\, e^{ik_c x} + c.c. + \mathscr{O}(A^3). \tag{4.52}$$

We have to include the spatial variations in the form

$$\frac{\partial}{\partial x} A(\mathbf{x},t) e^{ik_c x} = e^{ik_c x}\left(\frac{\partial}{\partial x} + ik_c\right)A(\mathbf{x},t),$$

$$\frac{\partial}{\partial y} A(\mathbf{x},t) e^{ik_c x} = e^{ik_c x}\frac{\partial}{\partial y} A(\mathbf{x},t). \tag{4.53}$$

This leads us to the expansion

$$(k_c^2 + \Delta) = \left(2ik_c\frac{\partial}{\partial x} + \frac{\partial^2}{\partial x^2} + \frac{\partial^2}{\partial y^2}\right)^2 \approx \left(2ik_c\frac{\partial}{\partial x} + \frac{\partial^2}{\partial y^2}\right)^2. \tag{4.54}$$

Here, we have taken into account that for slight spatial distortions of the stripe solution the second derivative in x-direction is small compared to the other terms.

Finally we end up with the so-called Newell-Whitehead-Segel equation

$$\partial_t A = \left[\varepsilon + 4k_c^2(\frac{\partial}{\partial x} - \frac{i}{2k_c}\frac{\partial^2}{\partial y^2})^2\right]A - 3A|A|^2. \tag{4.55}$$

Based on this equation, we can now calculate so-called *long wave instabilities* of the stripe patterns. To this end we consider stripe solutions characterized by the wave

number $\tilde{k} = k_c + k$

$$A = A_k e^{ikx} \tag{4.56}$$

and investigate small deviations

$$
\begin{aligned}
A &= A_k e^{ikx} + a_\kappa e^{ikx + i\kappa x} e^{\lambda t}, \\
A^* &= A_k^* e^{-ikx} + b_\kappa e^{-ikx + i\kappa x} e^{\lambda t}.
\end{aligned} \tag{4.57}
$$

It is convenient to introduce the abbreviation

$$G(\mathbf{k}) = \frac{1}{3}\left[\varepsilon - 4k_c^2 \left(k_x + \frac{1}{2k_c}k_y^2 \right)^2 \right]. \tag{4.58}$$

The linear eigenvalue problem takes the form

$$
\begin{aligned}
\lambda a &= [G(\mathbf{k} + \kappa) - 2G(\mathbf{k})]a - G(\mathbf{k})b, \\
\lambda b &= [G(\mathbf{k} - \kappa) - 2G(\mathbf{k})]b - G(\mathbf{k})a,
\end{aligned} \tag{4.59}
$$

and the characteristic equation reads

$$\lambda^2 - \lambda \operatorname{Tr}(A) - \operatorname{Det}(A) = 0, \tag{4.60}$$

where we have introduced trace and determinant of the matrix

$$A = \begin{pmatrix} G(\mathbf{k} + \kappa) - 2G(\mathbf{k}) & -G(\mathbf{k}) \\ -G(\mathbf{k}) & G(\mathbf{k} - \kappa) - 2G(\mathbf{k}) \end{pmatrix}. \tag{4.61}$$

$$
\begin{aligned}
\operatorname{Tr}(A) &= \lambda[G(\mathbf{k} + \kappa) + G(\mathbf{k} - \kappa) - 4G(\mathbf{k})], \\
\operatorname{Det}(A) &= G(\mathbf{k} + \kappa)G(\mathbf{k} - \kappa) - 2G(\mathbf{k} + \kappa)G(\mathbf{k}) - 2G(\mathbf{k} - \kappa)G(\mathbf{k}) \\
&\quad + 3G(\mathbf{k})^2.
\end{aligned} \tag{4.62}
$$

The solution is unstable provided $\operatorname{Det}(A) > 0$. Now, we can expand

$$G(\mathbf{k} \pm \kappa) = G(\mathbf{k}) \pm \kappa \nabla_k G(\mathbf{k}) + \frac{1}{2}(\kappa \cdot \nabla_k)^2 G(\mathbf{k}) + \dots. \tag{4.63}$$

This leads to

$$-(\kappa \cdot \nabla_k G(\mathbf{k}))^2 - G(\mathbf{k})(\kappa \cdot \nabla_k)^2 G(\mathbf{k}) > 0 \tag{4.64}$$

which can be turned into the condition

$$0 < G(\mathbf{k}) < -\frac{(\kappa \cdot \nabla_k G(\mathbf{k}))^2}{(\kappa \cdot \nabla_k)^2 G(\mathbf{k})}. \tag{4.65}$$

From this condition we can read off the existence of the two fundamental types of long wave instability of a pure stripe pattern with $k_y = 0$. In this case

$$\nabla_k G(\mathbf{k}) = -8k_c^2 k_x e_x, \qquad (\boldsymbol{\kappa} \cdot \nabla_k)^2 G(\mathbf{k}) = -8k_c^2 \kappa_x^2 \qquad (4.66)$$

and we obtain the following condition for instability

$$\varepsilon < 12k_c^2 k^2 = 3Dk^2 \qquad (4.67)$$

In the following we shall investigate by numerical solutions of the Swift-Hohenberg equation what actually will happen to stripe solutions, which are either *Eckhaus-* or *Zig-Zag-* unstable.

4.6.2.1 Zig-Zag Instability

As can be seen, straight rolls with $k < 0$, i.e. rolls with wavelength larger than the critical one, are unstable with respect to perturbations in transversal direction. This is the so-called Zig-Zag instability. The temporal development of a a stripe pattern, which is zigzag unstable, is exhibited in fig 4.5. Loosely speaking the stripes, which are too wide with respect to the critical wavelength try to decrease their wavelenght by forming zig-zag like patterns. The resulting patterns contain grain boundaries as well as defects, and exhibit a temporal evolution on a rather slow time scale

4.6.2.2 Eckhaus Instability

The next instability is the so-called Eckhaus instability. Stripes with wave lenght smaller than the critical one are unstable. Fig. (4.6) demonstrates the spatio-temporal evolution of an Eckhaus-unstable pattern. First, the amplitude of the pattern decreases so that defects can be generated. These defects eventually merge with the consequence that the wavelength of the stripes, which initially was in the Eckhaus unstable regime, returns to the Eckhaus-stable regime.

4.7 Hexagons

The Swift-Hohenberg equation (4.10) can be generalized by the inclusion of a quadratic nonlinearity [12, 13]. This has the consequence that hexagonal patterns become stable patterns in some parameter regions.

The numerical treatment of this equation demonstrates that it is possible to obtain hexagonal patterns in certain regions of the parameter space (ε, δ). An example is depicted in Fig. (4.7). Starting from random initial conditions we observe the formation of a hexagonal pattern. However, this pattern is not perfectly ordered. It contains defects, so-called penta-hepta defects consisting of a cell surrounded by seven respectively five neigbouring cells.
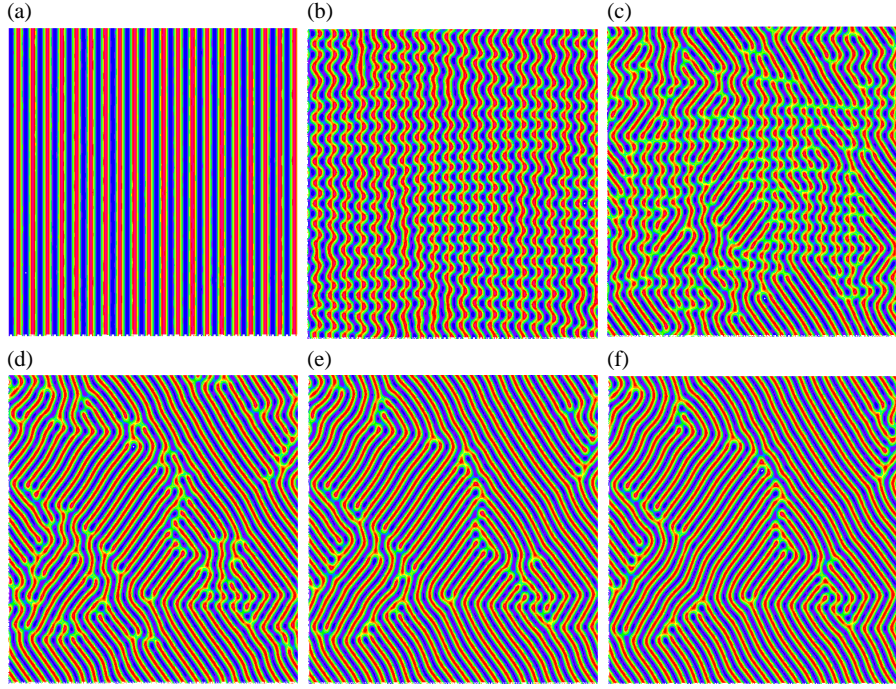
Fig. 4.5 Zig-zag Instability: Numerical Calculation of the evolution of stripe patterns from the Swift-Hohenberg equation (4.10) ($\delta = 0$, $\varepsilon = 0.3$). Initial conditions is a stripe pattern with wavelenght larger than the critical one plus small random deviations.

4.7.1 Stripes Versus Hexagons

The selection of hexagons versus stripes can be investigated on the basis of amplitude equations. In order to derive amplitude equations for the description of hexagons we perform the ansatz

$$\psi(\mathbf{x},t) = \xi_1 \, e^{i\mathbf{k}_1 \cdot \mathbf{x}} + \xi_2 \, e^{i\mathbf{k}_2 \cdot \mathbf{x}} + \xi_3 \, e^{i\mathbf{k}_3 \cdot \mathbf{x}} + c.c. \tag{4.68}$$

with the three wave vectors

$$\begin{aligned}
\mathbf{k}_1 &= k_c(1,0)\,, \\
\mathbf{k}_2 &= k_c\left(-\frac{1}{2}, \frac{\sqrt{3}}{2}\right), \\
\mathbf{k}_3 &= k_c\left(-\sqrt{\frac{1}{2}}, -\frac{\sqrt{3}}{2}\right).
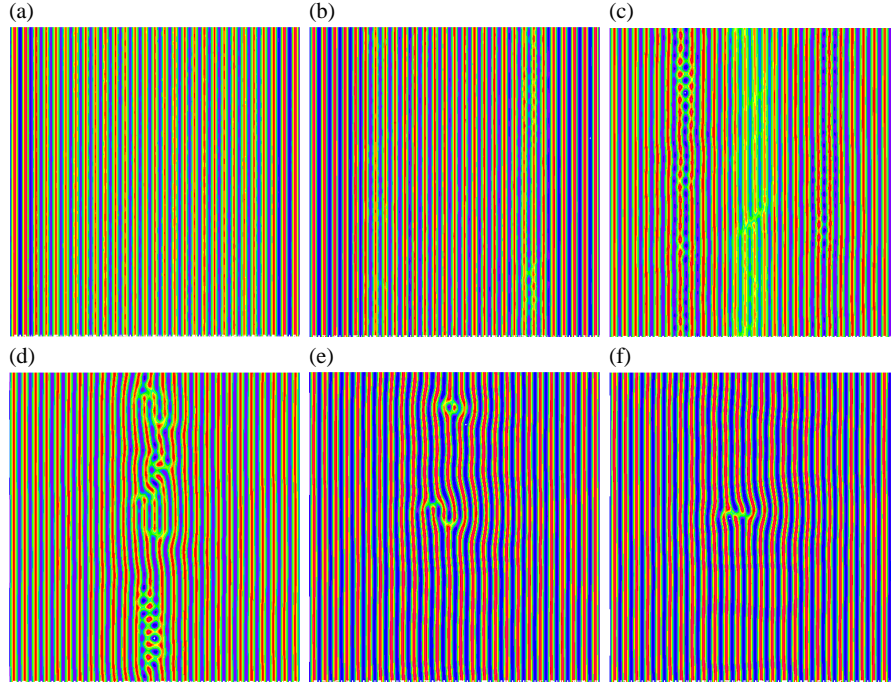\end{aligned} \tag{4.69}$$

Explicit calculation shows that

Fig. 4.6 Eckhaus-Instability: Numerical Calculation of the evolution of stripe patterns from the Swift-Hohenberg equation (4.10) ($\delta = 0$, $\varepsilon = .3$).

$$\psi(\mathbf{x},t)^2 = \xi_1^* \xi_2^* e^{-i(\mathbf{k}_1+\mathbf{k}_2)\mathbf{x}} + \xi_2^* \xi_3^* e^{-i(\mathbf{k}_1+\mathbf{k}_2)\mathbf{x}} + \xi_3^* \xi_1^* e^{-i(\mathbf{k}_1+\mathbf{k}_2)\mathbf{x}} + \dots . \quad (4.70)$$

Similar expressions arise for the cubic terms.

The resulting amplitude equations are obtained in a similar way as demonstrated for the stripe solutions:

$$
\begin{aligned}
\dot{\xi}_1 &= \varepsilon\xi_1 + \delta\xi_2^*\xi_3^* - \xi_1\left[a|\xi_1|^2 + b|\xi_2|^2 + b|\xi_3|^2\right] , \\
\dot{\xi}_2 &= \varepsilon\xi_2 + \delta\xi_3^*\xi_1^* - \xi_2\left[a|\xi_2|^2 + b|\xi_3|^2 + b|\xi_1|^2\right] , \\
\dot{\xi}_3 &= \varepsilon\xi_3 + \delta\xi_1^*\xi_2^* - \xi_2\left[a|\xi_3|^2 + b|\xi_1|^2 + b|\xi_2|^2\right] .
\end{aligned}
$$

$$(4.71)$$

The amplitude equations possess several types of solutions describing different types of patterns. The first type of solutions are the *stripes*. They are obtained from the ansatz

$$\xi_1 = \xi, \qquad \xi_2 = 0, \qquad \xi_3 = 0, \qquad (4.72)$$

where the amplitude ξ obeys the amplitude equation

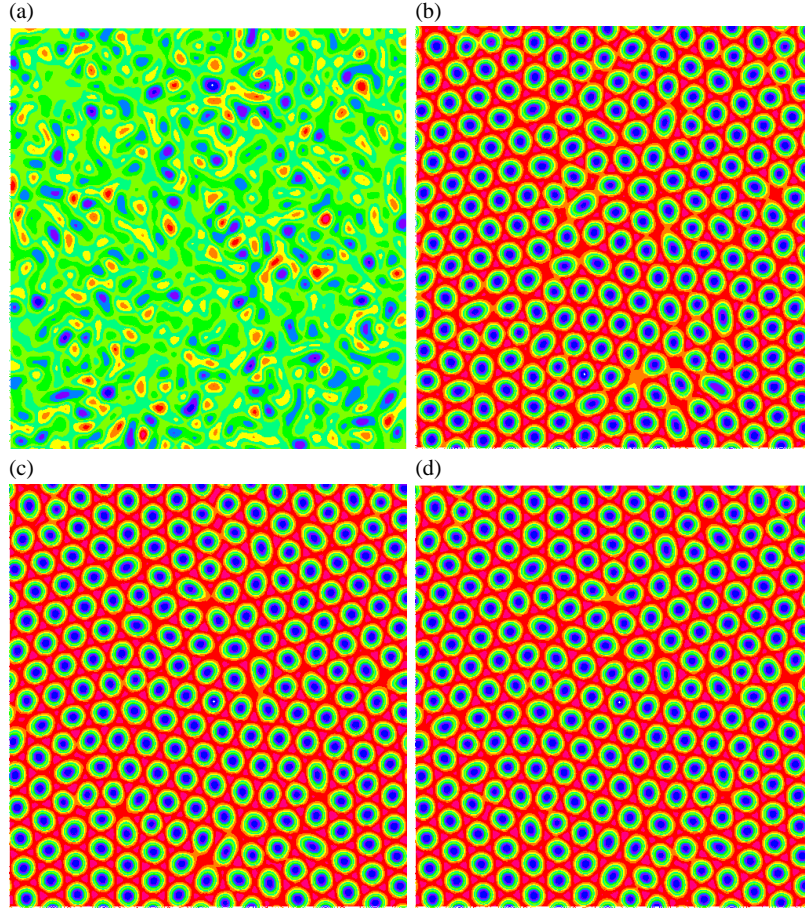$$\dot{\xi} = \varepsilon\xi - a\xi|\xi|^2. \qquad (4.73)$$

Fig. 4.7 Numerical calculation of the evolution of hexagonal patterns from the Swift-Hohenberg equation (4.10) ($\delta = 0.1$, $\varepsilon = 0.3$).

The solutions are

$$\xi = \sqrt{\frac{\varepsilon}{a}}\, e^{i\Phi}.$$

(4.74)

The phase Φ remains undetermined, which is due to the fact that the stripe pattern can be translated in space due to translational symmetry. The order parameter field $\psi(\mathbf{x}, t)$ takes the form

$$\psi(\mathbf{x}, t) = \sqrt{\frac{\varepsilon}{a}}\, \cos\left(\mathbf{k}_1 \cdot \mathbf{x} + \Phi\right)$$

(4.75)

and we explicitly see that change of the phase Φ corresponds to a shift of the pattern.

We consider now the stability analysis of the stripe solutions. To this end we introduce

$$\xi_1 = \xi + \eta_1, \qquad \xi_2 = \eta_2, \qquad \xi_3 = \eta_3 \tag{4.76}$$

and obtain the linear set of equations

$$\dot{\eta}_1 = -\varepsilon\eta_1 - \varepsilon\eta_1^*,$$
$$\dot{\eta}_2 = \varepsilon(1 - \frac{b}{a})\eta_2 - \delta\eta_3^*,$$
$$\dot{\eta}_3 = \varepsilon(1 - \frac{b}{a})\eta_3 - \delta\eta_2^*. \tag{4.77}$$

The characteristic equation determining the eigenvalue λ read

$$\lambda_{\pm} = \varepsilon(1 - \frac{b}{a}) \pm \delta. \tag{4.78}$$

The stripes are linearly stable for values of ε larger than

$$\varepsilon \leq \frac{\delta}{1 - \frac{b}{a}}. \tag{4.79}$$

Hexagon solutions are obtained by the ansatz

$$\xi_1 = \xi_2 = \xi_3 = A^{i\Phi} \tag{4.80}$$

which leads to the single amplitude equation

$$\dot{A} = \varepsilon A - \delta A^2 - A^3(a + 2b). \tag{4.81}$$

Nontrivial solutions are

$$A = -\frac{\delta}{2(a + 2b)} \pm \sqrt{\frac{\delta^2}{4(a + 2b)^2} + \varepsilon}. \tag{4.82}$$

There are further stationary solutions, the so-called *mixed mode solutions*.

We can summarize our discussions in Fig. 4.8, which exhibits the bifurcation diagram.

We mention that including slow spatial variations of the amplitudes $\xi_i(\mathbf{x}, t)$ according to the Newell-Whitehead-Segel theory allows one to determine the stability regions of stripes and hexagons with respect to long-wave instabilities as well as to investigate the detailed spatial structure of penta-hepta defects.
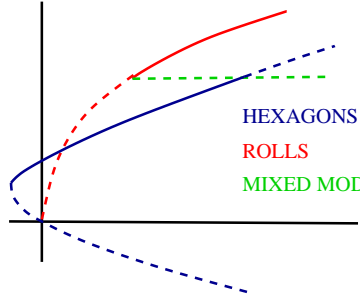
Fig. 4.8 Bifurcation diagram for stripes, hexagons

4.8 Nonvariational Effects and Pattern Formation

Up to now we have considered evolution equations for which a Ljapunov functional can be formulated. In this section, we consider extensions of the evolution equations, which do not have this important property. As a consequence, it can not expected in generality that the systems tend to stationary patterns with some optimal properties defined by the functional.

4.8.1 Model for Rotating Convection

A physically relevant system for a nonvariational system is convection in systems rotating about a vertical axis. Rotation breaks reflection symmetry. Due to the Coriolis force stripe patterns become unstable. This so-called Küppers-Lortz instability leads to spatially and temporally disordered patterns [35].

It has been shown that the following model equation for an order parameter field $\psi(\mathbf{x},t)$ is related to convection in rotating large aspect ratio systems [43, 42, 41] :

$$
\begin{aligned}
\partial_t \psi(\mathbf{x},t) = {}& \left[\varepsilon - (k_c^2 + \Delta)^2\right] \psi(\mathbf{x},t) - \alpha \left[\alpha \psi(\mathbf{x},t)^2 + (\nabla \psi(\mathbf{x},t))^2\right] \\
& + \nabla \cdot \left\{\nabla \psi(\mathbf{x},t) \left[\alpha \psi(\mathbf{x},t)^2 + (\nabla \psi(\mathbf{x},t))^2\right]\right\} \\
& - \mathrm{Ta}\beta \nabla \left\{ \times \mathbf{e}_z \times \nabla \psi(\mathbf{x},t) \left[\alpha \psi(\mathbf{x},t)^2 + (\nabla \psi(\mathbf{x},t))^2\right]\right\}.
\end{aligned} \tag{4.83}
$$

For $\mathrm{Ta} = 0$ we find the following Ljapunov functional

$$
V[\psi] = \int d\mathbf{x} \left[-\frac{1}{2}\{\varepsilon \psi^2 - \left[(k_c^2 + \Delta)\psi\right]^2\} + \frac{1}{4}\left[\alpha \psi^2 + (\nabla \psi)^2\right]^2 \right]. \tag{4.84}
$$

The evolution equation, therefore, has the general form

$$\dot{\psi} = -\frac{\delta}{\delta\psi}V - \mathrm{Ta}M[\psi] \tag{4.85}$$

By varying the Taylor number Ta, it is possible to gradually turn on non-variational effects.

4.8.1.1 Amplitude Equation

The ansatz

$$\psi(\mathbf{x},t) = \sum_{\mathbf{k}} A_{\mathbf{k}}(t)e^{i\mathbf{k}\cdot\mathbf{x}}, \qquad k = k_c = 1 \tag{4.86}$$

leads to the set of amplitude equations

$$\dot{A}_{\mathbf{k}} = \varepsilon A_{\mathbf{k}} - SA_{\mathbf{k}}|A_{\mathbf{k}}|^2 - A_{\mathbf{k}} \sum_{\mathbf{k}'\neq\mathbf{k}} (S + W_{\mathbf{k},\mathbf{k}'})|A_{\mathbf{k}'}|^2. \tag{4.87}$$

The straightforward calculation of the coefficients S, $W_{\mathbf{k},\mathbf{k}'}$ for the model equation yields

$$S = 3\alpha^2 + 2\alpha + 3,$$
$$W_{\mathbf{k},\mathbf{k}'} = S - 2 + 2\cos 2\Phi + 2\,\mathrm{Ta}\sin 2\Phi. \tag{4.88}$$

Here, Φ denotes the angle between the wave vectors $\mathbf{k}$, $\mathbf{k}'$.

4.8.1.2 Stripe Patterns

Roll solutions possess the amplitude

$$|A_{\mathbf{k}}|^2 = \frac{\varepsilon}{S}. \tag{4.89}$$

We consider now perturbations $A_{\mathbf{k}'}$ whose linear evolution is given by

$$\dot{A}'_{\mathbf{k}} = -\frac{\varepsilon}{S}W_{\mathbf{k}',\mathbf{k}}A_{\mathbf{k}}. \tag{4.90}$$

As a criterion for instability of rolls we obtain

$$W_{\mathbf{k},\mathbf{k}'} < 0. \tag{4.91}$$

4.8.1.3 Square Patterns

We first consider the case $\alpha = 0$. This case leads to the selection of square patterns. We explicitly obtain, considering the nonrotating case Ta $= 0$:

$$S = 3, \qquad W = 1 + 2\cos 2\Phi. \tag{4.92}$$

This indicates that rolls are unstable with respect to perturbations forming an angle larger than

$$\Phi = -\frac{1}{2}\arccos\frac{1}{2}. \tag{4.93}$$

The most unstable modes are disturbances with $\Phi = 90^\circ$, which indicates the selection of *square patterns*.

4.8.1.4 Küppers-Lortz Instability

Roll solutions possess the amplitude

$$|A_{\mathbf{k}}|^2 = \frac{\varepsilon}{S}. \tag{4.94}$$

We consider now perturbations $A_{\mathbf{k}'}$ whose linear evolution is given by

$$\dot{A}'_{\mathbf{k}} = -\frac{\varepsilon}{S}W_{\mathbf{k}',\mathbf{k}}A_{\mathbf{k}}. \tag{4.95}$$

As a criterion for instability of rolls we obtain

$$W_{\mathbf{k},\mathbf{k}'} < 0. \tag{4.96}$$

This gives us the condition

$$2\,\mathrm{Ta}\,\sin 2\Phi \geq S(\alpha) - 2 + 2\cos 2\Phi. \tag{4.97}$$

For each Taylor number, there is a critical angle, at which the instability sets in. This number is given by

$$\mathrm{Ta} = \frac{1}{\sin 2\Phi}\left[\frac{S}{2} - 1 + \cos 2\Phi\right]. \tag{4.98}$$

The minimum Taylor number is obtained for a critical angle Φ_c, which is calculated to be determined by

$$\frac{\partial}{\partial \Phi}\mathrm{Ta}(\Phi) = 0. \tag{4.99}$$

A straightforward calculation yields

$$\cos 2\Phi_c = -\frac{2}{S-2} \tag{4.100}$$

and the corresponding critical Taylor number is

$$\mathrm{Ta}_c = \sqrt{(S/2-1)^2 - 1} = \sqrt{\frac{S^2}{4} - S}. \tag{4.101}$$

We can now determine the value of α, which corresponds to the critical angle of $60°$. This yields

$$\cos 120° = -\frac{1}{2} = -\frac{2}{S-2}. \tag{4.102}$$

This is achieved for the value

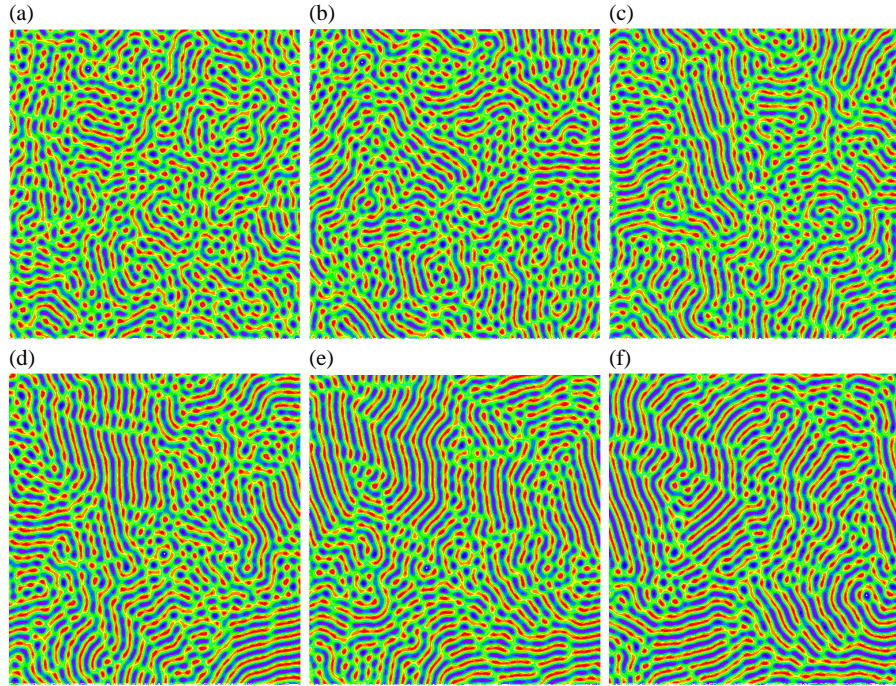$$\alpha_{60} = \frac{1 + \sqrt{10}}{3} \approx 1.38. \tag{4.103}$$

Fig. 4.9 Numerical Calculation of the evolution of patterns exhibiting a Küppers-Lortz type instability.

4.8.2 Model for Spiral Turbulence

A highly interesting pattern forming process can be detected in Rayleigh-Bénard convection in fluids which are characterized by a low Prandtl number, i.e. by a small ratio of kinematic viscosity and heat conductivity. These fluids are only slightly viscous but can well conduct heat. The low viscosity of the fluid has the consequence that vortical motions, i.e. nearly two dimensional fluid motions in the horizontal plane, are only slightly damped and can interfere with the dynamics of the convection rolls. This has the consequence that in addition to the order parameter field $\psi(\mathbf{x},t)$ a vortical velocity field has to be taken into account.

We denote the vortical flow (quite often also denoted as *mean flow*) by $\mathbf{V}(\mathbf{x},t)$. Since the mean flow is two dimensional it can be derived from a stream function $\chi(\mathbf{x},t)$. As is well-known the stream function of a two dimensional flow obeys the evolution for the stream function

$$\dot{\Delta}\chi(\mathbf{x},t) + \frac{\partial}{\partial x}\Delta\chi\frac{\partial}{\partial y}\chi(\mathbf{x},t) - \frac{\partial}{\partial x}\chi\frac{\partial}{\partial y}\Delta\chi(\mathbf{x},t) = f(\mathbf{x},t)\,. \tag{4.104}$$

External forcing is included in terms of $f(\mathbf{x},t)$. The stream function is a secondary order parameter field, which is forced by convective motion.

A detailed analysis performed in [39, 38] leads to a generalization of the Swift-Hohenberg equation including a *mean flow*

$$\dot{\psi}(\mathbf{x},t) + \mathbf{u}(\mathbf{x},t)\cdot\nabla\psi(\mathbf{x},t) = \left[\varepsilon - (k_c^2 + \Delta)^2\right]\psi(\mathbf{x},t) + N\left[(\mathbf{x},t)\right]\,,$$
$$\mathbf{u}(\mathbf{x},t) = -\nabla\times\mathbf{e}_z\chi(\mathbf{x},t)\,,$$
$$\dot{\Delta}\chi = [-\gamma + \Delta]\Delta\chi + \delta\mathbf{e}_z\cdot[\nabla\psi(\mathbf{x},t)\times\nabla\Delta\psi(\mathbf{x},t)]\,. \tag{4.105}$$

The vortical motion is assumed to be weak so that nonlinearities in the equation for the stream function can be neglected. The coupling between the two fields is the transport of the convective rolls due to vortical motion on the one hand side and excitation of fluid motion by convection [39, 38].

4.8.2.1 Giant Spirals

We can generate giant spiral solutions using a circular domain and the boundary conditions

$$\psi_{\delta V} = d\,, \qquad \chi = 0\,. \tag{4.106}$$

For more information we refer the reader to [5].

4.8.2.2 Spiral Defect Turbulence

Figure 4.10 exhibits the spatio-temporal evolution of patterns generated by the model equation (4.105). For further details we refer to [4].
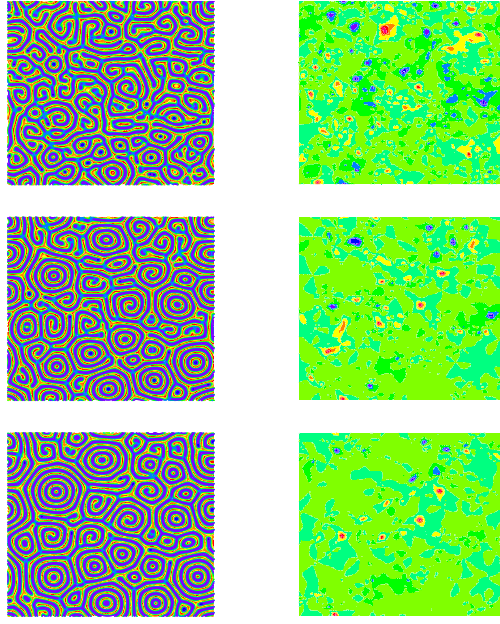
Fig. 4.10 Numerical Calculation of the evolution of patterns resembling spiral defect turbulence in Rayleigh- Bénard systems. The left side shows the order parameter field, which has to be identified with the temperature field. The right side exhibits the stream function χ related with the vortical motion in the plane.

4.9 Complex Swift-Hohenberg Equations

It is well-known that nonequilibrium systems are capable of generating selfsustained temporal oscillations.

A generic mechanism for the emergence of such oscillations is the so-called Hopf-bifurcation. A simple extension can be based on the amplitude equation, where we now assume that the linear growth rate is complex

$$\dot{\xi}_{\mathbf{k}} = \left[\varepsilon + i\omega_0 + ib(k_c^2 - \mathbf{k}^2) - (1+ia)(k_c^2 - \mathbf{k}^2)^2 \right] \xi_{\mathbf{k}} . \qquad (4.107)$$

This linear relation indicates that the mode amplitudes grow with the growth rate $\varepsilon - (k_c^2 - \mathbf{k}^2)^2$ in an oscillatory way, where the frequency is

$$\omega = \omega_0 + b(k_c^2 - \mathbf{k}^2) - a(k_c^2 - \mathbf{k}^2)^2 . \qquad (4.108)$$

The linear field takes the form

$$\psi(\mathbf{x}, t) = \sum_{\mathbf{k}} \frac{e^{i(\mathbf{k}\cdot\mathbf{x} - \omega t)} e^{\lambda_r(k)t}}{\sqrt{V}} \xi_{\mathbf{k}} + \frac{e^{i(\mathbf{k}\cdot\mathbf{x} + \omega t)} e^{\lambda_r(k)t}}{\sqrt{V}} \xi_{\mathbf{k}} . \qquad (4.109)$$

It is a superposition of traveling waves traveling in $\mathbf{k}$ and $-\mathbf{k}$ direction. A superposition of right and left traveling waves may also lead to standing waves.

In addition to the mechanisms of saturation of the amplitudes and the selection of patterns the nonlinearity now controls the selection of traveling waves versus standing waves. The following complex order parameter equation has been used to investigate these questions in some details:

$$
\begin{aligned}
\partial_t \psi(\mathbf{x},t) = {} & \left[\varepsilon + i\omega i\alpha \left(k_c^2 + \Delta \right) - (1+ia)\left(k_c^2 + \Delta \right)^2 \right] \psi(\mathbf{x},t) \\
& - A |\psi(\mathbf{x},t)|^2 \psi(\mathbf{x},t) - B |\nabla \psi(\mathbf{x},t)|^2 \psi(\mathbf{x},t) \\
& - C \left(\nabla \psi(\mathbf{x},t) \right)^2 \psi(\mathbf{x},t)^* .
\end{aligned}
\tag{4.110}
$$

For details we refer to the publications [14, 7, 9, 10, 11, 8]